Journal of
Plankton Research

plankt.oxfordjournals.org

J. Plankton Res. (2016) 38(2): 290–304. First published online January 13, 2016 doi:10.1093/plankt/fbv108

Costa Rica Dome: Flux and Zinc Experiments

Biological response of Costa Rica Dome phytoplankton to Light, Silicic acid and Trace metals

JOAQUIM I. GOES[1]*, HELGA DO ROSARIO GOMES[1], KAREN E. SELPH[2] AND MICHAEL R. LANDRY[3]

[1]LAMONT DOHERTY EARTH OBSERVATORY AT COLUMBIA UNIVERSITY, PALISADES, NEW YORK, NY 10964, USA, [2]DEPARTMENT OF OCEANOGRAPHY, UNIVERSITY OF HAWAII AT MANOA, HONULULU, HI 96822, USA AND [3]SCRIPPS INSTITUTION OF OCEANOGRAPHY, UNIVERSITY OF CALIFORNIA AT SAN DIEGO, 9500 GILMAN DR, LA JOLLA, CA 92093, USA

*CORRESPONDING AUTHOR: jig@ldeo.columbia.edu

Received May 31, 2015; accepted November 19, 2015

Corresponding editor: John Dolan

The Costa Rica Dome (CRD) is a unique open-ocean upwelling system, with picophytoplankton dominance of phytoplankton biomass and suppressed diatoms, yet paradoxically high export of biogenic silica. As a part of Flux and Zinc Experiments cruise in summer (June–July 2010), we conducted shipboard incubation experiments in the CRD to examine the potential roles of Si, Zn, Fe and light as regulating factors of phytoplankton biomass and community structure. Estimates of photosynthetic quantum yields revealed an extremely stressed phytoplankton population that responded positively to additions of silicic acid, iron and zinc and higher light conditions. Size-fractioned Chl *a* yielded the surprising result that picophytoplankton, as well as larger phytoplankton, responded most to treatments with added silicic acid incubated at high incident light (HL + Si). The combination of Si and HL also led to increases in cell sizes of picoplankton, notably in *Synechococcus*. Such a response, coupled with the recent discovery of significant intracellular accumulation of Si in some picophytoplankton, suggests that small phytoplankton could play a potentially important role in Si cycling in the CRD, which may help to explain its peculiar export characteristics.

KEYWORDS: picophytoplankton; nanophytoplankton; microphytoplankton; *Synechococcus*; silicic acid; light

INTRODUCTION

The Costa Rica Dome (CRD) is a seasonal upwelling feature located at the eastern end of the thermal ridge that separates the westward North Equatorial Current (NEC) and the eastward North Equatorial Counter Current (NECC) (Fiedler, 2002). It generally forms around 9°N and 90°W in early spring when the eastward moving NECC impinges on the coast of Central America and deflects northwards causing a redistribution of mass (Wyrtki, 1964). Although there is disagreement as

available online at www.plankt.oxfordjournals.org

to the exact physical processes responsible for the formation of the CRD (Hofman *et al.*, 1981; Umatani and Yamagata, 1991), Fiedler (Fiedler, 2002) has shown that the CRD is a seasonal phenomenon that originates in mid-spring along the coast of Costa Rica and subsequently strengthens under the influence of local wind-driven divergence and cross-current flow.

During its active phase in summer, cyclonic circulation and thermocline shoaling make CRD surface waters generally cooler and richer in inorganic nutrients compared with adjacent waters of the eastern Equatorial Pacific (EEP). Although typical in some respects to other tropical upwelling regions, one unique feature of the CRD is its exceptionally rich and diverse community of picophytoplankton, dominated by *Synechococcus* (SYN) (Li *et al.*, 1983; Saito *et al.*, 2005; Gutiérrez-Rodríguez *et al.*, 2014), whose cell numbers exceed 1×10^6 cells mL^{-1} (Li *et al.*, 1983) and are among the highest recorded for the global oceans (Ahlgren *et al.*, 2014). The dominance of SYN in the CRD is in stark contrast to the nearby Peruvian upwelling system (Bruland *et al.*, 2005), where diatom biomass exceeds that of SYN by 1–2 orders of magnitude.

Conditions that support the remarkably high densities of SYN populations, while simultaneously suppressing diatoms in the CRD are not well understood (Ahlgren *et al.*, 2014). It is known that cobalt (Co), an essential element for SYN growth (Sunda and Huntsman, 1995; Saito and Moffett, 2002), is present in exceptionally high concentrations in the CRD as ligand-bound compounds that are easily accessible to SYN (Saito *et al.*, 2005). An on-deck incubation experiment conducted by Saito *et al.* (Saito *et al.*, 2005) also confirmed that Fe was important for SYN growth. Cell densities of SYN responded dramatically when Fe was added with Co, leading the authors to conclude that SYN was co-limited by Co and Fe. In a subsequent study, based mainly on hydrographic and nutrient relationships in the CRD, Ahlgren *et al.* (Ahlgren *et al.*, 2014) concluded that a combination of newly upwelled macronutrients, a warm and shallow mixed layer, high concentrations of Co and a scarcity of Fe and Mn all contributed to creating a special niche for SYN, that is not well suited for diatom growth. In that latter regard, one shipboard grow-out experiment conducted by Franck *et al.* (Franck *et al.*, 2003) in August 2000 indicated that large eukaryotic phytoplankton in the CRD were limited by Fe and Zn. Zn in particular is chelated by strong ligands in seawater (Bruland, 1989; Lohan *et al.*, 2002), making it less available to diatoms and other larger taxa (Leblanc *et al.*, 2005).

In addition or in combination with Fe or Zn, it is possible that low Si could be a limiting resource for diatoms or other phytoplankton in the CRD, as noted previously in the EEP (Ku *et al.*, 1995; Leynaert *et al.*, 2001). As in other HNLC regions, diatoms growing at low concentrations of Fe in the EEP have relatively high Si:Nitrate drawdown ratios (Hutchins and Bruland, 1998; Takeda, 1998), leading to Fe and Si co-limitation of diatom growth in the EEP (Brzezinski *et al.*, 2008, 2011). Baines *et al.* (Baines *et al.*, 2011) showed that while Fe limited the growth of diatoms in the EEP, cell volumes and cellular Si contents of diatoms increased significantly with Si additions. Given the dominance of picophytoplankton (notably SYN) in the CRD, along with the recent discovery of significant Si concentration in SYN cells (Baines *et al.*, 2012), we hypothesize that Si may be broadly important as a limiting resource for smaller as well as larger phytoplankton groups in this region.

As a part of Flux and Zinc Experiments cruise in summer (June–July 2010), we conducted shipboard incubation experiments to examine the potential roles of Si, Zn, Fe and light as regulating factors of phytoplankton biomass and community structure in the CRD. Prior to our cruise, no studies have examined the potential role of Si as a regulator of phytoplankton communities in the CRD. Cobalt was excluded from these experiments because it is present in high concentrations in the CRD (Ahlgren *et al.*, 2014).

METHOD

Cruise details

Experiments were performed on board R/V *Melville* from 21 June to 22 July 2010, during the summer period when the CRD upwelling is generally most intense. During the summer 2010, however, surface temperatures in and around the CRD (>27°C) were higher than normal and the sky was overcast much of the time, the aftermath of moderate El Niño conditions earlier in the year. Although there have been no previous reports describing the role of El Niño events on the CRD, the surface expression of the dome in terms of chlorophyll *a* (Chl *a*) concentrations was substantially weaker than observed in any other summer period over the decade from 2004 to 2014 (Landry *et al.*, 2016a), and satellite coverage in general was poor. As a consequences, we used transect sampling to locate the central dome region of minimal temperature at 20 m (Fig. 1). Relative to the central dome area, several sites were selected for process studies (termed "Cycles") of 4–5 days duration following the path of a satellite-tracked surface drifter with a holey-sock drogue centered at 15 m (Fig. 1).

Each cycle involved a coordinated series of water-column sampling and process experiments to assess changes in hydrography and composition of the plankton community (Freibott *et al.*, 2016; Gutiérrez-Rodríguez *et al.*, 2016;

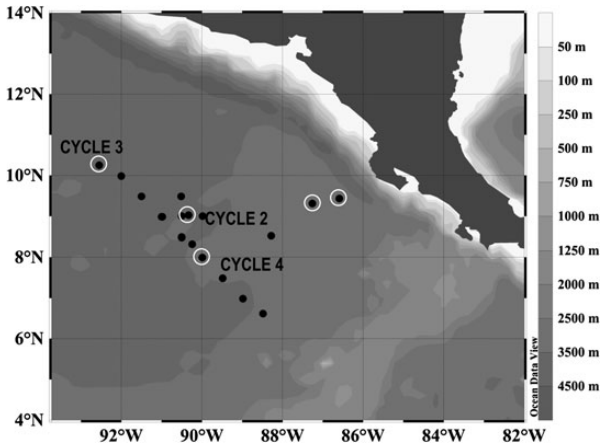

Fig. 1. Map of study region, showing transect (black dots) and cycle stations (encircled black dots). Incubation experiments were undertaken at Cycles 2, 3 and 4.

Landry *et al.*, 2016a; Taylor *et al.*, 2016), micro- and mesozooplankton grazing, biogenic silica production and material export (Décima *et al.*, 2016; Krause *et al.*, 2016; Landry *et al.*, 2016b; Stukel *et al.*, 2016). Here, we report the results of shipboard grow-out experiments undertaken during Cycles 2, 3 and 4 (Fig. 1). Cycles 2 and 4 (~9°N, 90°W and ~8°N, 90°W, respectively) were located within the dome as evident by the presence of cooler and denser waters and the shoaling of isotherms. Cycle 3 was located in an open-ocean site at the northwest edge of the dome.

Sample collection

At each cycle location (Fig. 1), water samples for the grow-out experiments were acquired from a single depth in the water column, usually in the morning of the first day. Prior to collection of the seawater samples, a Kimoto® *in situ* FRRF equipped with a Biospherical® Instruments Inc. scalar Irradiance sensor (QS2200) (Fujiki *et al.*, 2011) was used to profile photosynthetically active radiation (PAR) and the distribution of phytoplankton biomass in the water column, and to establish the photosynthetic competency of cells through measurements of variable fluorescence (Fv/Fm) and σPSII. The former is a measure of the maximum quantum yield of photochemistry in PSII and characterizes the efficiency of primary photosynthetic reactions; the latter is an estimate of the functional absorption cross-section of PSII. The maximum value of Fv/Fm is ~0.65 in healthy algae and usually decreases under stress conditions (Kolber and Falkowski, 1993). Fv/Fm profiles were utilized to determine the depth from which the natural communities were sampled for the experiments. Our criteria were that the phytoplankton community had to be from the upper mixed layer with a reasonably high Chl *a* concentration (>0.5 mg L^{-1}), but also show signs of stress (Fv/Fm <0.4) as discernible from the Fv/Fm profiles to ensure positive response to nutrient additions over the course of the experiments. Using these criteria, we initiated experiments with water collected from 12, 20 and 15 m, for Cycles 2, 3 and 4, respectively.

Sample collection for the experiments was undertaken with a SeaBird® trace metal clean rosette, equipped with a CTD sensor and eight 5-L Niskin bottles with external Teflon-coated springs. When the rosette was back on deck after water collection, the Niskin bottles were detached, taken into a class 100 "clean" van and kept under positive pressure with HEPA-filtered air. The bottles were first sampled for initial concentrations of Zn, Fe and Si, and then gently drained under low light into several sets of pre-cleaned 1-L Nalgene® polycarbonate bottles for the grow-out experiments described below. Pre-cleaning of the bottles involved 3 weeks of soaking in 10% trace metal-free HCl, followed by several rinses with deionized water.

Immediately after the trace metal clean cast, seawater samples taken from an independent Niskin cast were used to estimate nitrate (NO_3), nitrite (NO_2), phosphate (PO_4) and silicic acid [$Si(OH)_4$] concentrations in the water column. Nutrient samples were immediately frozen and analyzed later at the nutrient laboratory of the University of California, Santa Barbara on a Lachat Instruments QuikChem® 8000 (Gordon *et al.*, 1992).

Additionally, total Chl *a* (whole water), as well as nano (2–20 μm) and picophytoplankton (<2 μm) Chl *a*, were estimated from several depths in the upper ~45 m of the water column. For total Chl *a* analysis, duplicate sets of whole water samples (250 mL) were filtered onto 25 mm Whatman® GF/F filters (nominal pore size 0.7 μm). The filters were immediately transferred into disposable cuvettes containing 10 mL of acetone. Chl *a* was extracted at −20°C in the dark for 24 h. The extracts were vortex mixed, brought to room temperature in the dark, and quantified in a pre-calibrated Turner Designs® model-10 fluorometer. To estimate Chl *a* in size fractions, duplicate samples from each depth were pre-filtered through a 20 μm pore size Nucleopore® filter. The filtrates were collected in a clean flask, and 250 mL samples of each were then filtered through 25 mm Whatman® GF/F filters. Chl *a* captured on this filter (<20 μm) was extracted and measured as described above. The rest of the <20 μm filtrate was further prefiltered through a 2 μm pore size Nucleopore® filter, then collected on a GF/F filter to estimate picoplankton (PICO, <2 μm). Chl *a* attributable to the nanophytoplankton (NANO, 2–20 μm) fraction was computed as the difference between Chl *a* values in the <2 and

<20 μm fractions. Chl *a* attributable to microplankton (MICRO, >20 μm) was calculated as the difference between Total Chl *a* and the <20 μm fractions.

To aid in understanding the effects of Si, Zn, Fe and PAR as regulators of phytoplankton community structure in the CRD, we conducted two types of experiments. The first set conducted during Cycles 2, 3 and 4 focused on the synergistic effects of PAR and Si on phytoplankton community composition and biomass, whereas the second set during Cycle 3 was aimed at understanding the individual effects of Si, Fe and Zn on phytoplankton communities of the CRD.

Silicic acid and light experiments

For the light and Si amendment experiments, we quantified phytoplankton responses in terms of: (i) two size fractions of Chl *a* (PICO and NANO + MICRO) and (ii) flow cytometric (FCM) measurements of cell abundances of *Prochlorococcus* (PRO), *Synechococcus* (SYN), picoeukaryotes (PEUK) and nano + microeukaryotes (MICRO-EUK) and associated parameters such as Forward Light Scatter (FLS), Side Scatter (SS), cellular Chl *a* and DNA content. FCM analyses for SYN, PEUK and MICRO-EUK were undertaken within 30 min of sample collection using a Beckman-Coulter® XL, equipped with a 15 mW 488 nm argon ion laser and an Orion® syringe pump to deliver 2.2 mL samples at a rate of 0.44 mL min^{-1}. Fluorescence signals were normalized to 1.0 μm yellow–green (YG) polystyrene beads (Polysciences® Inc., Warrington, PA, USA). Listmode data files (FCS 2.0 format) of cell fluorescence and light-scatter properties were acquired with System II software (Beckman-Coulter) and further processed using FlowJo® software (Tree Star, Inc., www.flowjo.com).

Because the shipboard FCM was not sensitive enough to detect dim PRO populations, additional subsamples for FCM were preserved (0.5% paraformaldehyde, v/v, final concentration) and frozen in liquid nitrogen on shipboard, and stored at −80°C until shore-based analysis. The samples were thawed and stained with Hoechst 33342 (1 μg mL^{-1}, v/v, final concentration) at room temperature in the dark for 1 h (Monger and Landry, 1993). Aliquots (100 μL) were analyzed using a Beckman-Coulter EPICS® Altra Flow Cytometer with a Harvard Apparatus syringe pump for volumetric sample delivery. Simultaneous (co-linear) excitation of the plankton was provided by two water-cooled 5 W argon ion lasers, tuned to 488 nm (1 W) and the UV range (200 mW). The optical filter configuration distinguished populations on the basis of Chl *a* (red fluorescence, 680 nm), phycoerythrin (orange fluorescence, 575 nm), DNA (blue fluorescence, 450 nm) and forward and 90° side scatter signatures. Calibration beads (0.5 and 1.0 μm yellow–green beads and 0.5 μm UV beads) were used as fluorescence standards. Listmode files were collected using Expo32 software (Beckman-Coulter), and then processed using the FlowJo software.

The stock solution of Si for the experiments was prepared using Fisher® reagent grade $Na_2SiO_3 \cdot 9H_2O$ in trace metal-free water. To remove trace metal contaminants, the solution was acidified to pH 2 with Sigma-Aldrich® trace metal-free HCl, carefully passed through a 20 cm column containing the sodium form of the Chelex-100 chelating resin prepared using the method of Davey *et al.* (Davey *et al.*, 1970) and then collected in trace metal-free Teflon (Nalgene®) bottles. The sodium form of the Chelex resin is superior to the hydrogen- or the ammonium-preconditioned resins as a trace metal absorbent, and it is also less prone to ammonium contamination (Davey *et al.*, 1970). Our analysis of the Si-stock in an auto-analyzer revealed no nitrate, nitrite or ammonium contamination.

Duplicate bottles containing 1 L seawater from the trace metal cast were prepared for each of the following conditions: (i) HL−Control incubated at 100% of ambient light with no Si addition (ambient light refers to PAR measured at depth of sample collection); (ii) HL + Si (incubated at 100% of ambient light and spiked with 4 μM Si); (iii) LL−Si (incubated at 20% of ambient light and no Si addition); (iv) LL + Si (incubated at 20% of ambient light and spiked with 4 μM Si).

After the amendments, the bottles were immediately transferred into a plexiglass incubation tank and covered with neutral density screens to simulate PAR at the depths of sample collection. Incident light in the deck incubator was measured with a Biospherical Instruments® QSL 100 sensor. Temperature was regulated with continuously flowing sea water drawn from ~3 m below the surface. For the LL treatments, individual bottles were placed in neutral density socks to further reduce light to ~20% of ambient levels.

Trace metal and silicic acid amendment experiments

For the trace metal and Si amendment experiments conducted during Cycle 3, duplicate sets of seawater samples from the trace metal cast were amended as follows:

(1) +2 nM Zn (added as zinc chloride);
(2) +5 nM Fe (added as ferric chloride);
(3) +4 μM Si; and
(4) Control (no micro or macro- nutrient additions).

Control and amended samples were quickly transferred into the deck incubator covered with neutral density

screening to bring light close to ambient levels. In this experiment, both the control and the treated samples were incubated under ambient light (HL) only. As soon as the bottles were transferred to the incubation tanks, subsamples of seawater from the trace metal cast were filtered for initial measurements (Day 0) of whole, PICO- and NANO + MICRO Chl *a*. In addition to size-fractionated measurements of Chl *a*, changes in PRO, SYN and PEUK and MICRO-EUK were monitored using FCM analyses.

After Day 0, the bottles were sampled every second day, at approximately the same time of the day, for 8 days (10 days in the case of the trace metal and Si experiments). Two experimental bottles from each treatment were removed from the incubation tank and sampled for Chl *a* and FCM analysis, as described above.

Previous studies have cautioned against running on-deck incubations beyond 48 h, especially for small volume incubation bottles (<250 mL), as experimental results could potentially be confounded by "bottle effects". However, it has been shown that "bottle effects" can be greatly reduced in long-term incubation experiments through the use of larger incubation vessels (Li and Harrison, 1982). Olson *et al.* (Olson *et al.*, 2000), Lam *et al.* (Lam *et al.*, 2001), Tortell *et al.* (Tortell *et al.*, 2002), Lam *et al.* (Lam *et al.*, 2001) and more recently Ryan-Keogh *et al.* (Ryan-Keogh *et al.*, 2013) all used larger bottles (≥1 L) and were able to observe significant stimulation of photosynthesis and growth rates without the loss of cell integrity in on-deck incubation experiments even in those extending beyond 48 h. For our experiments, we used 1 L polycarbonate bottles, and even after 6 days, we were able to observe substantial phytoplankton growth as increase in Chl *a* and cell numbers, with no loss in cell integrity as seen in FCM-derived cellular DNA content.

Statistical analyses

Tests for significance of differences in size-fractioned Chl *a* between the control and treated samples in the grow-out experiments were done using the repeated measures analysis of variance test available in SigmaPlot® ver.13, which allows for multi-pairwise comparisons of group means. This analysis was restricted to data from Days 2 to 6, to minimize potential bottle artifacts over long incubations. Before the statistical tests were undertaken, the data were tested for normality and equality of their variance distribution. All data sets that passed these tests were tested for differences in the mean values among the treatment groups using the Holm–Sidak pairwise multiple comparison procedure. Data sets that failed the normality test were tested using the Friedman repeated measurements analysis of variance test on ranks.

RESULTS

Environmental characteristics of the three experimental cycles

Hydro-chemical and biological features during each cycle experiment are described in detail elsewhere in this issue (Landry *et al.*, 2016; Selph *et al.*, 2016; Taylor *et al.*, 2016). At each location, SSTs varied narrowly between 27.5 and 27.8°C with the lowest value measured in Cycle 4 (Fig. 2a–c). Mixed-layer depths were very shallow (12 m) at the start of Cycles 2 and 4 (Fig. 2a and c) and ~24 m in Cycle 3 (Fig. 2b). Average mixed-layer $NO_3 + NO_2$ concentrations were 2.5 μM in Cycle 2 (Fig. 2a) and 1.4 and 1.7 μM (Fig. 2b and c) in Cycles 3 and 4, respectively. Below the thermocline, NO_3 concentrations were in excess of 24 μM for all three cycles. Dissolved PO_4 concentrations in Cycles 2, 3 and 4 were 0.4, 0.3 and 0.3 μM, respectively, in the mixed layer (Fig. 2a–c) and ~1.9 μM below the thermocline. Average mixed layer values for Si were slightly higher (3.3 μM) in Cycle 2 (Fig. 2a) when compared with Cycles 3 and 4 (2.5 and 2.9 μM, respectively) (Fig. 2b and c). Mixed-layer concentrations of Zn and Fe were very low for all cycles (Vedamati, 2013; Chappell *et al.*, 2016).

Fluorescence profiles (FL) indicative of Chl *a* distribution in the water column during Cycles 2 and 4 show prominent subsurface fluorescence maxima (SSFM) at 32 and 38 m, respectively, below the mixed layer and in the vicinity of the nutricline (Fig. 3a and c). Cycle 3, however, lacked a well-developed SSFM (Fig. 3b). In all three cycles, Fv/Fm profiles (Fig. 3a–c) reveal nutrient-stressed phytoplankton (values of ≤0.4) in the mixed layer, as well as in the SSFM. FRRF-derived σPSII measurements were highest in phytoplankton just below the sea surface, a sign of the reduced light harvesting potential of resident phytoplankton cells. Interestingly the highest values of Fv/Fm (≥0.5) occurred below the SSFM, indicative of phytoplankton populations whose growth rates were in balance with the supply of nutrients. These features of FRRF profiles were consistent across the three cycles.

Average mixed-layer concentrations of total Chl *a* were highest for Cycle 2 (0.28 ± 0.02 mg m^{-3}), compared with 0.23 ± 0.03 and 0.16 ± 0.01 mg m^{-3} for Cycles 3 and 4, respectively. Within the SSFM, total Chl *a* concentrations were 0.46 and 0.31 mg m^{-3} for Cycles 2 and 4, respectively (Fig. 4a and c) and 0.27 mg m^{-3} for Cycle 3 which lacked a prominent subsurface maximum (Fig. 4b).

Microphytoplankton accounted for a minor fraction of phytoplankton community Chl *a* in the mixed layer for all three cycles (Fig. 4a–c), except for Cycle 2 at 30 m where it accounted for ~36% (~0.18 mg m^{-3} Chl *a*) of total Chl *a*. In contrast, PICO accounted for 60% of total

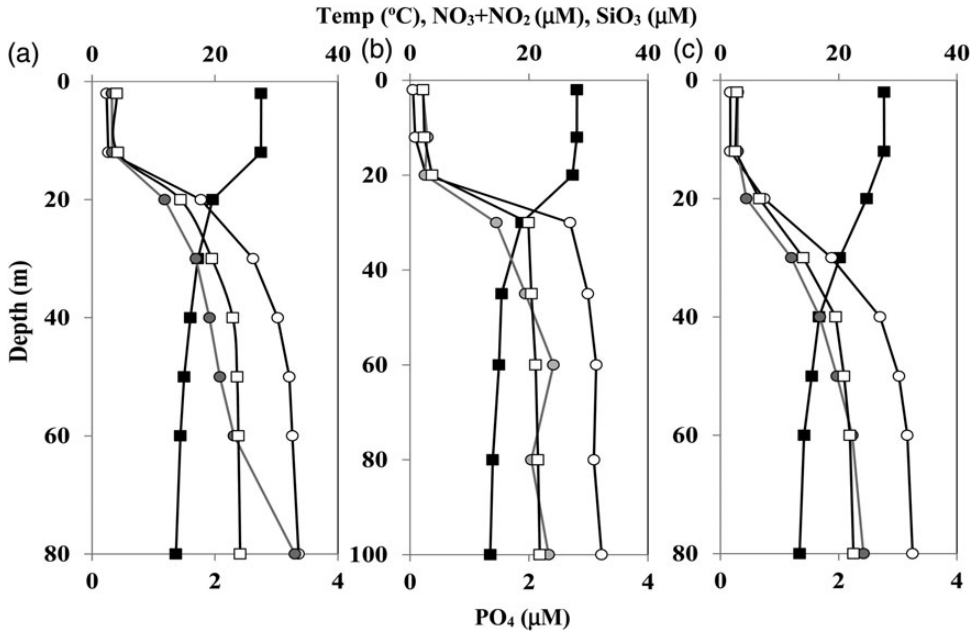

Fig. 2. Depth profiles of seawater temperature (°C), inorganic nitrate + nitrite, phosphate and silicic acid (all µM) at the start of (**a**) Cycle 2, (**b**) Cycle 3 and (**c**) Cycle 4.

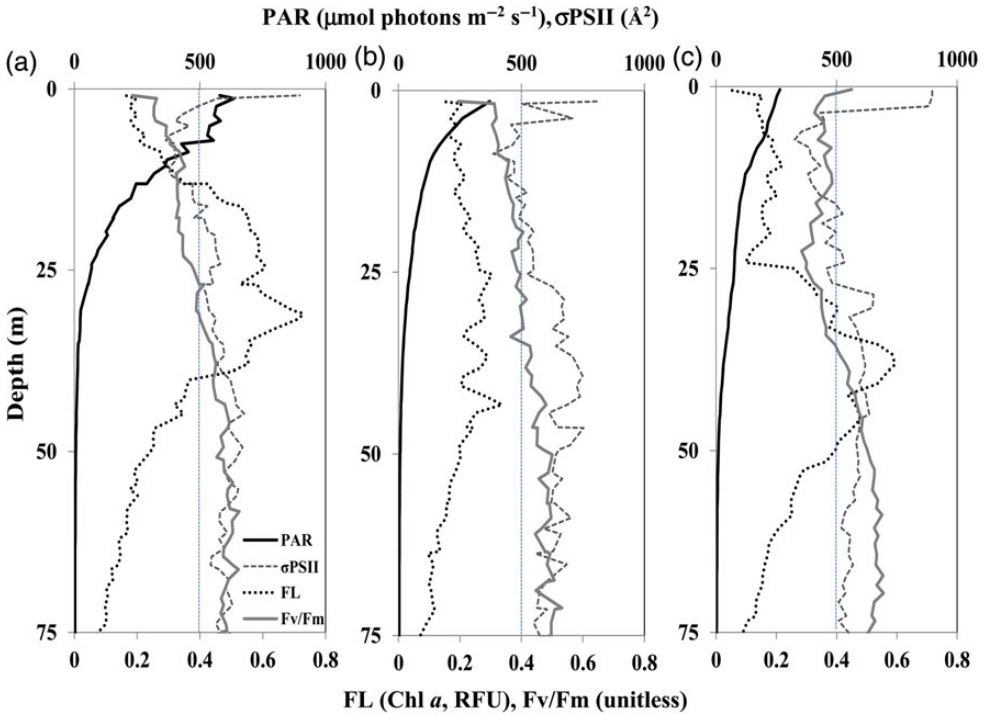

Fig. 3. Depth profiles of PAR (µmol m^{-2} s^{-1}), Fv/Fm (unitless), σPSII (Å) and fluorescence (FL, Relative Fluorescence Units, proxy for Chl *a*). Fv/Fm values of 0.4 in the water column are depicted by the vertical dashed line.

Chl *a* in Cycle 2. In Cycle 3, MICRO accounted for <1% of total Chl *a*, which comprised roughly equal amounts of nano- and picophytoplankton. In Cycle 4, MICRO made up almost 72% of total Chl *a* just above the SSFM, but above and below the SSFM, Chl *a* concentrations were dominated by NANO and PICO.

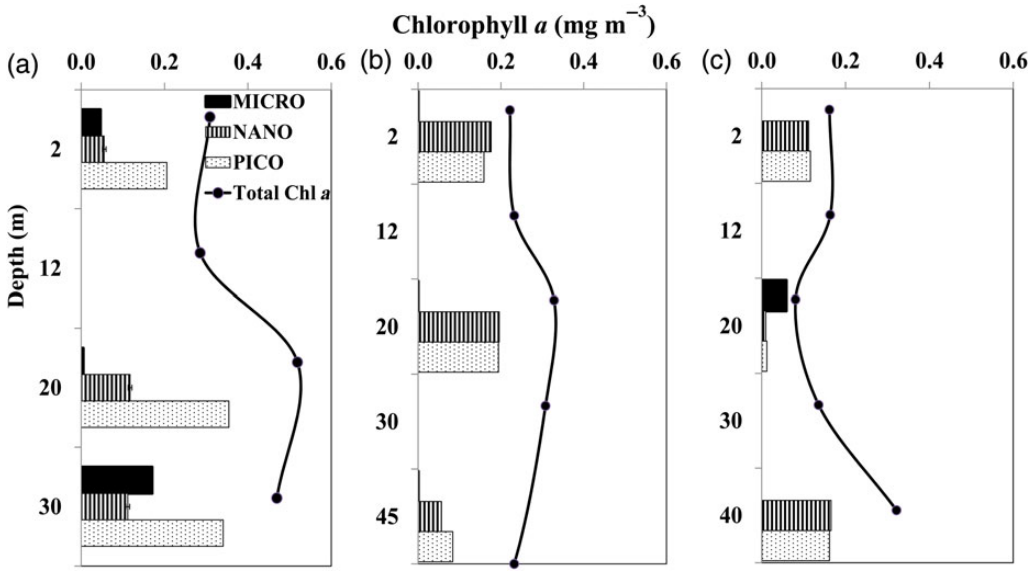

Fig. 4. Depth profiles of whole water sample chlorophyll *a* (Total Chl *a*) and Chl *a* within the picoplankton, nanoplankton and microplankton fractions. All values in mg m^{-3}.

Ambient cell abundances of PRO (~2.2 × 10^3 cells mL^{-1}) did not vary appreciably among the three cycles. In contrast, SYN abundances varied >2-fold, from 2.7 × 10^3 cells mL^{-1} in Cycle 2 to 6.8 × 10^3 cells mL^{-1} in Cycle 3, with intermediate values of 5.0 × 10^4 cells mL^{-1} in Cycle 4. Total EUK abundances, including PICO, NANO and MICRO-eukaryotes, showed moderate (<2-fold) variability, with lowest values for Cycle 4 (0.85 × 10^4 cells mL^{-1}), highest for Cycle 3 (1.50 × 10^4 cells mL^{-1}) and intermediate for Cycle 2 (1.15 × 10^4 cells mL^{-1}) (Taylor *et al.*, 2016).

Si enrichment and light amendment experiments

Incident light levels measured at noon each day in the deck incubators varied from 125 to 1250 μmol m^{-2} s^{-1}. This wide range reflected the day-to-day differences in cloud cover, some days being exceptionally cloudy or cloud-free. Results of Si and light amendment experiments are presented in Figs 5–8, and the pair-wise *t*-tests for significance of differences between treatments are given in Tables I and II.

Cycle 2 results

Samples from Cycle 2 incubated in HL, with and without Si addition, showed the most conspicuous increase in PICO Chl *a*, particularly in the HL + Si-treated samples from 0.15 mg m^{-3} on Day 0 to 0.48 mg^{-3} by Day 6 (Fig. 5a). By Day 8, PICO Chl *a* concentrations were 0.82 mg m^{-3}. Differences between the HL + Si-treated samples and the LL + Si and LL − Con samples were statistically significant at $P \leq 0.1$ (Table I). Differences were also observed in PICO Chl *a* between the HL + Si and the HL − Con samples (Fig. 5a), but these differences were not statistically significant. The NANO + MICRO fraction showed similar results to the PICO-fraction, with the Chl *a* increase in the HL + Si-treated samples being significantly greater than the LL-Con and the LL + Si treatments (Fig. 5b, Table I).

During Cycle 2, PRO concentrations increased almost 4-fold from 2.5 × 10^3 cells mL^{-1} on Day 0 to 9.2 × 10^3 cells mL^{-1} on Day 2 in the Hi + Si-treated samples, declining thereafter (Fig. 5c). *Prochlorococcus* concentrations also increased in the HL-Con treatment from Day 0 to Day 2 by ~1.6-fold, declining on Day 4 but increasing to 7.1 × 10^4 cells mL^{-1} on Day 6. For SYN, the highest increase was observed on Day 2 in the HL-Con-treated samples, where cell concentrations doubled to 5.4 × 10^4 from 2.7 × 10^3 cells mL^{-1} on Day 0 (Fig. 5d). In comparison, the increase in SYN in the HL + Si samples, as well as in the LL + Si and the LL-Con treatments, was marginal. PEUK cell abundances increased in the HL + Si-treated samples from 1.12 × 10^4 on Day 0 to 3.5 × 10^4 cells mL^{-1} on Day 6 (Fig. 5e). However, differences between the HL + Si and the other treatments were not statistically significant (Table II). For MICRO-EUK also, the largest increase from Day 0 cell numbers of 0.4 × 10^4 cells mL^{-1} was recorded on Day 6 (1.8 × 10^4 cells mL^{-1}) in the HL + Si-treated samples, and MICRO-EUK cell concentrations

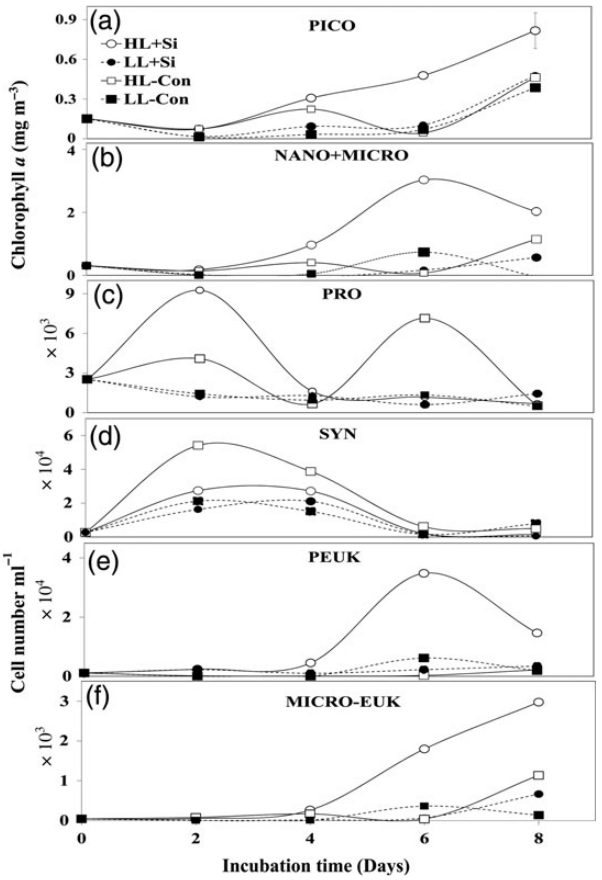

Fig. 5. Changes in (**a**) picoplankton Chl *a* and (**b**) nano + microplankton Chl *a* during on-deck grow-out experiments with seawater samples from Cycle 2. Samples were treated as follows: (i) ambient light + silicic acid (HL + Si), (ii) low light + silicic acid (LL + Si), (iii) ambient light-control (HL-Con) and (iv) low light-control (LL-Con). Error bars indicate standard deviation of duplicate measurements. (**c**) *Prochlorococcus* (PRO), (**d**) *Synechococcus* (SYN) and (**e**) picoeukaryotes (PEUK) and (**f**) nano + microeukaryotes (MICRO-EUK) from Cycle 2. Samples were treated as follows: (i) ambient light + silicic acid (HL + Si), (ii) low light + silicic acid (LL + Si), (iii) ambient light-control (HL-Con) and (iv) low light-control (LL-Con).

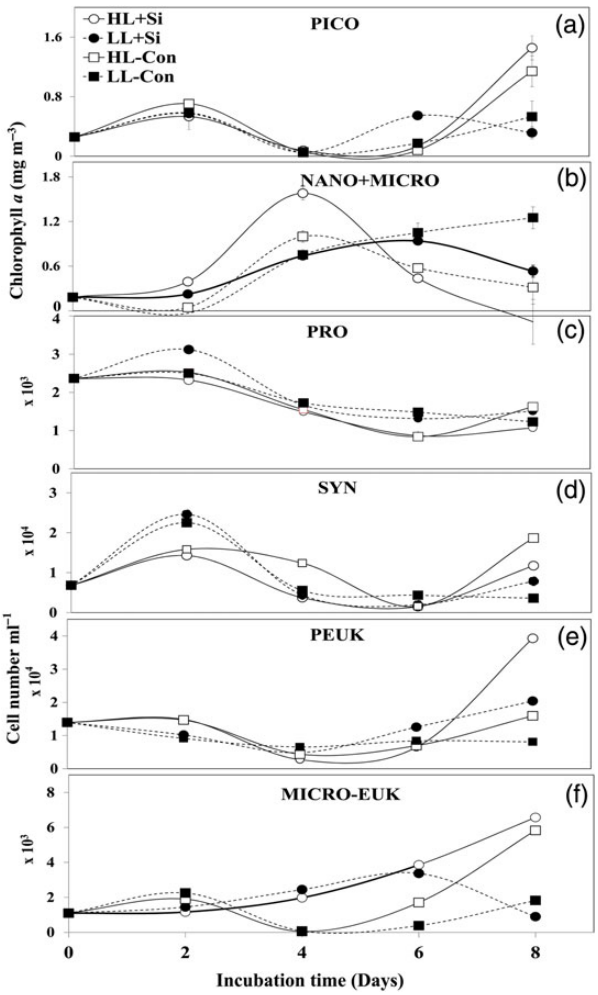

Fig. 6. Same as in Fig. 5, but with seawater from Cycle 3.

reached 2.9×10^4 cells mL^{-1} on Day 8 (Fig. 5f). MICRO-EUK increases in the other treatments were marginal (Fig. 5f). Despite perceptible differences among treatments, especially for PRO, PEUK and MICRO-EUK, these differences were not statistically significant.

FCM measurements of FLS, SS, Chl *a* and DNA accompanying the changes in cell numbers during Cycle 2 showed little change over the course of the experiments, with two notable exceptions. First, for both PRO and SYN populations, large increases in relative SS (SS-treatment versus SS-control) were observed in the HL + Si treatments (i.e. 4.1 on Day 4 for PRO, and 4.4 on Day 6 for SYN). In comparison, increases in relative SS for the eukaryotic phytoplankton populations under HL + Si were modest. Secondly, for the low light + Si experiments, the SYN, PEUK and MICRO-EUK populations showed increased relative Chl *a* fluorescence in +Si treatments versus controls.

Cycle 3 results

During Cycle 3, the most perceptible increase in PICO Chl *a* occurred in the HL + Si and the HL-Con samples but only by Day 8 (Fig. 6a). Chl *a* increases from 0.26 mg m^{-3} on Day 0 were modest during the first 6 days in all treatments but rose to 1.46 mg m^{-3} in the HL + Si and 1.14 mg m^{-3} in the HL-Con treatments by Day 8. With the exclusion of Day 8 from the statistical testing, treatment differences were not significant (Table I).

Changes in NANO + MICRO Chl *a* were clearly the highest in the HL + Si treatment, increasing from 0.18 mg m^{-3} on Day 0 to 1.58 mg m^{-3} by Day 4, and declining thereafter (Fig. 6b). NANO + MICRO Chl *a*

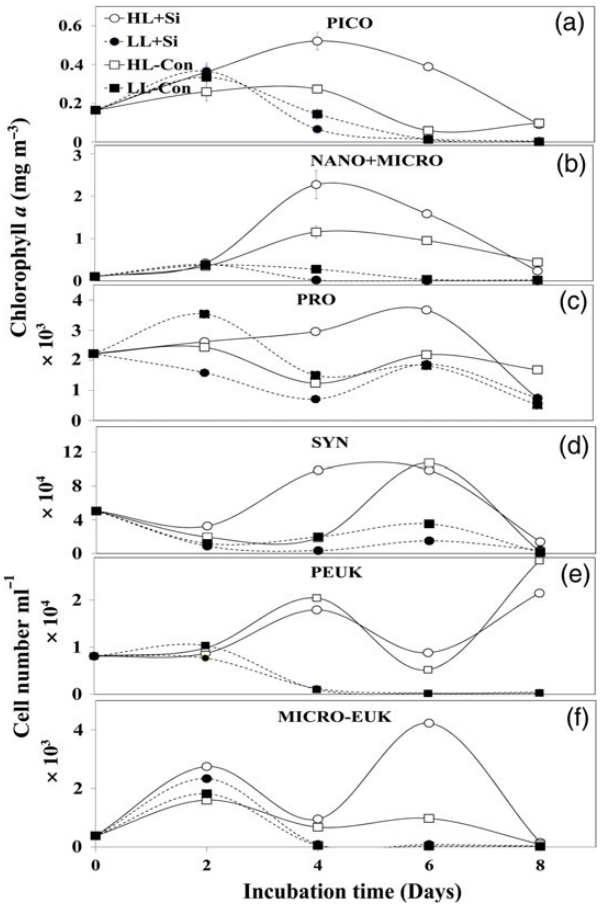

Fig. 7. Same as in Fig. 5, but with seawater from Cycle 4.

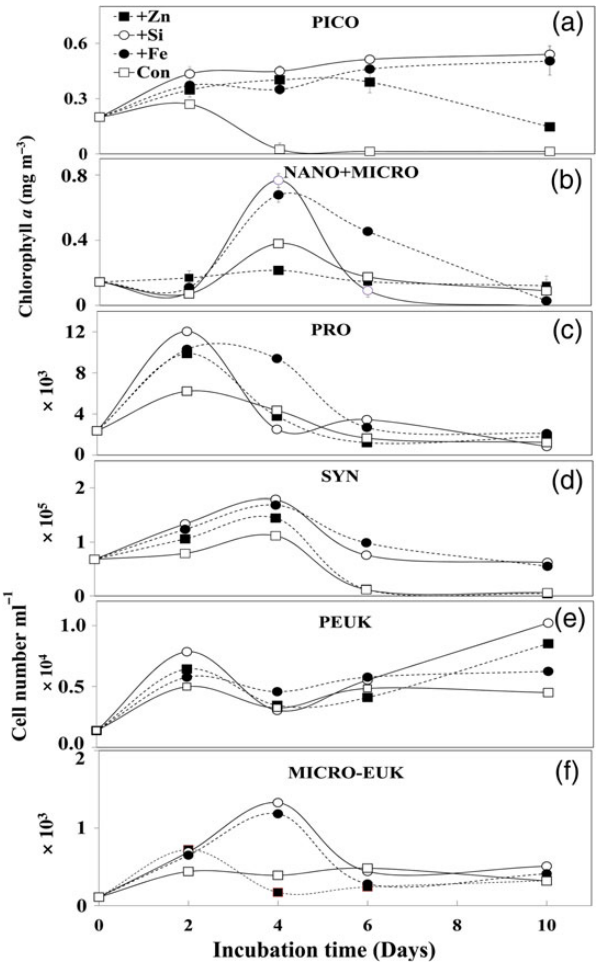

Fig. 8. Changes in (**a**) picoplankton Chl *a*, (**b**) nano + microplankton Chl *a*, (**c**) PRO, (**d**) SYN and (**e**) PEUK and (**f**) MICRO-EUK during on-deck grow-out experiments incubated under ambient light with seawater samples from Cycle 3 and amended as follows: (i) +5 nM Fe, (ii) +2 nM Zn, (iii) +4 μM Si and (iv) un-amended control (Con).

also increased in the HL-Con treatment by Day 4. In the case of LL + Si, the greatest increase in NANO + MICRO Chl *a*, from 0.18 mg m^{-3} on Day 0 to 0.93 mg m^{-3}, was observed on Day 6, declining thereafter. The other treatment which with a conspicuous increase in NANO + MICRO Chl *a* was LL-Con. Differences between all the treatments were, however, not significant (Table I).

The largest changes in PRO cell numbers were observed on Day 2 in all the treatments, but were highest in the LL + Si treatment (Fig. 6c). Thereafter, by Day 6, PRO abundances declined in all the treatments. SYN cells also increased in all the treatments by Day 2 and were highest in the LL-Con and LL + Si samples (Fig. 6d), declining thereafter. PEUK cell numbers showed the largest change in the HL + Si increasing from 1.42×10^4 cells mL^{-1} on Day 0 to 3.93 cells mL^{-1} by Day 8 (Fig. 6e). Differences in the treatments for SYN and PEUK were not significant (Table II). For MICRO-EUKs, cell numbers increased by Day 2 in all treatments, but were highest in the HL + Si treatment (Fig. 6f). The other noticeable increase in MICRO-EUK cell numbers was observed for the HL-Con.

Changes in the ratios of FCM cellular characteristics between the treatments and the controls again revealed an ∼3-fold increase in relative FLS and∼29-fold increase in relative SS for SYN in the HL + Si treatment.

Cycle 4 results

For the Cycle 4 experiment, PICO Chl *a* in the HL + Si treatment increased from 0.18 on Day 2 to 0.52 mg m^{-3} by Day 4, but tapered off thereafter (Fig. 7a). Modest increases were also observed for other treatments, but, unlike the observations in the dome during Cycle 2, increases in PICO Chl *a* between the treatments were not statistically significant (Table I). NANO + MICRO Chl *a* increases were greatest in the Hi + Si treatment by Day

Table I: Noon time values of PAR and results of the paired t*-tests depicting the significance of differences in picoplankton Chl* a *and nano + microplankton Chl* a *between Control, Si and light-treated samples from experiments at Cycles 2–4 and from trace metal experiments (TME) at Cycle 3*

	Cycle 2			Cycle 3			Cycle 4			TME			
	125–1029 μE m^{-2} s^{-1}			600–1209 μE m^{-2} s^{-1}			240–1252 μE m^{-2} s^{-1}			600–1209 μE m^{-2} s^{-1}			
Noon-time PAR Treatment	HL-Con	HL + Si	LL-Con	HL-Con	HL + Si	LL-Con	HL-Con	HL + Si	LL-Con	Treatment	Zn	Fe	Si
Picoplankton													
HL + Si	0.13			0.63			0.11			Fe	0.34		
LL-Con	0.19	0.042[a]		0.37	0.43		0.35	0.13		Si	0.13	0.018[a]	
LL + Si	0.54	0.043[a]	0.09	0.67	0.63	1.00	0.63	0.63	0.70	Con	0.13	0.030[a]	0.016[a]
	HL-Con	HL + Si	LL-Con	HL-Con	HL + Si	LL-Con	HL-Con	HL + Si	LL-Con		Zn	Fe	Si
Nano + Microplankton													
HL + Si	0.18			0.61			0.26			Fe	0.34		
LL-Con	0.56	0.072[a]		0.37	0.75		0.09[a]	0.09[a]		Si	0.68	0.46	
LL + Si	0.19	0.096[a]	1.00	0.42	0.99	0.50	0.1[a]	0.13	0.63	Con	0.79	0.22	0.65

Grey-shaded values indicate data that failed the normality and equal variance tests. Data for Days 0 and 8 were excluded from this analysis.
[a]A significant difference at $P < 0.1$ level.

Table II: Noon time values of PAR and results of the repeated measures ANOVA depicting the significance of differences in Prochlorococcus, Synechococcus *and eukaryotes between Control, Si and light-treated samples from experiments at Cycles 2–4 and from trace metal experiments (TME) at Cycle 3*

	Cycle 2			Cycle 3			Cycle 4			TME			
	125–1029 mE m^{-2} s^{-1}			600–1209 mE m^{-2} s^{-1}			240–1252 mE m^{-2} s^{-1}			600–1209 μE m^{-2} s^{-1}			
Noon-time PAR Treatment	HL-Con	HL + Si	LL-Con	HL-Con	HL + Si	LL-Con	HL-Con	HL + Si	LL-Con	Treatment	Zn	Fe	Si
Prochlorococcus													
HL + Si	0.98			0.63			0.63			Fe	0.22		
LL-Con	0.24	0.35		1.00	0.071[a]		0.94	0.38		Si	1.00	0.52	
LL + Si	0.34	0.63	0.83	0.20	0.036[a]	0.41	0.019[a]	0.083[a]	1.00	Con	1.00	0.13	1.00
	HL-Con	HL + Si	LL-Con	HL-Con	HL + Si	LL-Con	HL-Con	HL + Si	LL-Con		Zn	Fe	Si
Synechococcus													
HL + Si	0.13			0.13			0.30			Fe	0.63		
LL-Con	0.13	0.16		0.57	0.75		0.34	0.072[a]		Si	0.13	0.13	
LL + Si	0.18	0.50	0.63	0.63	0.57	0.67	0.27	0.13	0.19	Con	0.008[a]	0.13	0.91
	HL-Con	HL + Si	LL-Con	HL-Con	HL + Si	LL-Con	HL-Con	HL + Si	LL-Con		Zn	Fe	Si
Picoeukaryotes (PEUK)													
HL + Si	1.00			1.00			0.48			Fe	0.97		
LL-Con	0.57	0.14		0.40	0.41		0.14	0.63		Si	0.63	0.45	
LL + Si	0.14	0.13	0.43	0.56	0.53	0.28	0.11	0.13	0.49	Con	0.32	0.012[a]	0.18
	HL-Con	HL + Si	LL-Con	HL-Con	HL + Si	LL-Con	HL-Con	HL + Si	LL-Con		Zn	Fe	Si
Nano plus microeukaryotes (N + MEUK)													
HL + Si	0.63			0.30			0.20			Fe	0.37		
LL-Con	0.48	0.17		0.22	0.17		0.27	0.19		Si	0.16	0.58	
LL + Si	0.22	0.15	0.75	0.85	1.00	0.42	0.61	0.23	0.13	Con	0.74	0.36	0.59

Values that have been shaded failed the normality and equal variance tests. Data for Days 0 and 8 were excluded from this analysis.
[a]Significant difference at the $P < 0.1$ level.

4, and a modest increase was observed in the HL-Con samples also by Day 4 (Fig. 7b), declining thereafter. Differences in treatments for NANO + MICRO Chl *a* were statistically significant between HL + Si and the LL-Con and between HL-Con and LL-Con and LL + Si (Table II).

The most noticeable changes in PRO cell numbers were observed by Day 2 in the LL + Si treatment and by Day 4 in the HL + Si treatment (Fig. 7c). SYN numbers also responded positively to the HL + Si treatment, and cell numbers were highest by Day 4 (Fig. 7d) and significantly greater than the changes observed in the LL-Con treatment. PEUK cell abundances changed only marginally by Day 2 in all the treatments, but increased by Day 4 in the HL + Si and HL-Con samples. A decline in PEUK abundance was observed by Day 6, but increases

occurred thereafter in both HL + Si and HL-Con treatments. Changes in PEUK cell numbers in the LL + Si and the LL-Con were marginal by Day 2 and declined from Day 4 onwards (Fig. 7e). For MICRO-EUKs, highest cell abundances were recorded on Day 6 for HL + Si (Fig. 7f). MICRO-EUK changes in other treatments were marginal, but surprisingly they were not significantly different from the HL + Si treatment (Table II).

FCM-derived cell characteristics once again revealed an almost 3-fold increase in relative SS for SYN by Day 6. Changes in FCM parameters for other phytoplankton groups were at best marginal during this experiment.

Trace metal and Si enrichment experiment

The impacts of Zn, Fe and Si additions on PICO Chl *a* were obvious by Day 2 of the experiment, with values in the trace metal and Si-amended samples >0.40 mg m^{-3} compared with <0.26 mg m^{-3} in the control (Fig. 8a). PICO Chl *a* continued to increase in the +Zn, +Fe and +Si-treated samples through Days 4 and 6, but only marginally compared with the doubling of Chl *a* on Day 2. The largest increase in picophytoplankton Chl *a* was observed in the +Si sample, which was significantly different from the Co samples but not statistically different from the +Zn and +Fe treatments (Table I).

Changes in NANO+MICRO Chl *a* were most significant for the +Si and +Fe treatments, with values reaching concentrations of 0.77 and 0.68 mg Chl *a* m^{-3}, respectively, by Day 4 (Fig. 8b). By Day 6, however, NANO + MICRO Chl *a* declined in all bottles.

Changes in PICO Chl *a* in the +Zn, +Si and +Fe treatments on Day 4 (Fig. 8a) were accompanied by 4-fold increases in PRO relative to Day 0 (Fig. 8c). Thereafter, PRO densities declined rapidly, except for the +Fe treatment. Consistent with the observed increases in PICO Chl *a*, SYN abundances were also highest on Day 4 in the +Si, +Zn and +Fe-amended samples compared with the controls (Fig. 8d), with only the +Zn-treated sample showing a statistically significant difference at $P < 0.1$ level. PEUK cell numbers increased from 0.1×10^4 cells mL^{-1} on Day 0 to $>0.5 \times 10^4$ cells mL^{-1} by Day 2 in all treatments, with the highest abundances in the +Zn and +Si treatments. After Day 4, the largest increases in the PEUK fraction were observed on Day 10 in the +Zn and +Si treatments (Fig. 8e). For MICRO-EUK cell numbers increased in all treatments on Day 2, with the highest abundance (1.1×10^3 cells mL^{-1}) on Day 4 in the +Fe samples (Fig. 8f).In this experiment, the most obvious positive changes in FCM cell parameters over the controls were observed in the relative magnitude of SS for PEUK in the +Si and +Fe-treated samples, and increased CHL/cell for all groups in the +Fe samples.

DISCUSSION

Summer 2010 was an unusual year for the CRD. During the preceding winter, when the CRD generally starts appearing close to the Central American coast, the Ocean Niño Index indicated a moderate El Niño event. By time that our cruise was underway, however, the conditions were rapidly transitioning to La Niña-like conditions (Landry *et al.*, 2016a). Not much is known about how such ENSO swings impact the evolution and growth of the CRD, but 2010 does stand out as a summer of atypically low surface expression of satellite SST and Chl *a* relative to surrounding waters (Landry *et al.*, 2016a). Among the areas sampled for the present study, mixed-layer depths for sites closest to the dome center (Cycles 2 and 4) were shallower than on the dome edge (Cycle 3), but mixed-layer nutrient concentrations and trace metal concentrations (Chappell *et al.*, 2016; Vedamati, 2013) were uniformly low for all three cycle.

The combination of low Fv/Fm coupled with high σPSII values in the surface mixed layer throughout the cruise were indicative of phytoplankton populations with suboptimal growth rates and cellular photo-physiological properties (Fig. 3a–c). Subsurface populations (within the first 10 m) were particularly characterized by extremely low Fv/Fm and high values of σPSII even during FRRF casts undertaken at dawn, suggesting severe nutrient and trace metal limitation (Vassiliev *et al.*, 1995; Suggett *et al.*, 2009), as opposed to the more typical photo-inhibition of surface phytoplankton populations in tropical oligotrophic waters. Additionally, for most of our study, the sky was overcast, ruling out the possibility that surface phytoplankton populations in the CRD were photo-inhibited. Generally speaking, smaller phytoplankton, such as SYN, PRO and smaller diatoms, are likely less prone to photo-inhibition because of their reduced pigment absorption cross-sections (Kana and Glibert, 1987; Key *et al.*, 2010). In our incubations, we also observed consistently higher rates of Chl *a* accumulation for HL-treated samples, suggesting that PAR during our cruise was not at photo-inhibitory, but limiting levels. These observations are consistent with the findings of Gutiérrez-Rodríguez *et al.* (Gutiérrez-Rodríguez *et al.*, 2016), who observed highly significant increases in the growth rates of SYN and pico-EUK when natural populations of these organisms growing under LL conditions within the SSFM were transplanted to HL conditions at the surface. Consistent with previous observations, SYN concentrations were relatively higher during our cruise, possibly the result of the CRD's elevated Co concentrations (Saito *et al.*, 2005) together

with the CRD's unique hydrographic and nutrient conditions (Ahlgren *et al.*, 2014).

With the exception of the study by Franck *et al.* (Franck *et al.*, 2003), who showed that deficiencies in Zn and Fe could limit Si uptake by diatoms, no other studies have examined why diatoms are poorly represented in the CRD. Consistent with those previous results, the addition of Fe in our experiments had a substantial positive impact on Chl *a* accumulation in the NANO + MICRO fraction. In contrast to their findings, however, the addition of Zn did not lead to any appreciable increase in Chl *a* for larger phytoplankton, although it did enhance PICO Chl *a*. FCM data also indicated enhanced PICO Chl *a* and associated increases in cell numbers of PRO, SYN and PEUK in the +Si, +Zn and +Fe treatments. Although these differences were not always statistically significant, Zn and Si additions led to the largest increases in PICO Chl *a* relative to the controls. Increases in NANO + MICRO Chl *a* in the +Si and +Fe treatments were also observed in the FCM data for the MICRO-EUK size fraction.

We observed that the effectiveness of Si as a stimulant for different phytoplankton communities was greatly enhanced when natural populations were grown under HL conditions than under reduced light conditions. Size-fractionated Chl *a* measurements during the three grow-out experiments revealed higher biomass accumulation (and therefore, higher net growth rates) in the HL + Si-treated samples for both the nano + micro and picoplankton fractions. Microscopic observations of a few experimental samples fixed with 1% Lugol's iodine and preserved in 1.5% buffered formaldehyde under a Nikon® inverted microscope revealed that the NANO + MICRO phytoplankton fraction was made up largely of 10−20 μm pennate diatoms, of the genus *Pseudo-nitzschia*.

During all three light and Si amendment experiments, FCM measurements revealed a net positive effect of the HL + Si treatment on SYN growth. The most interesting observation was that of a dramatic increase in SYN cell size indicated by the enhancement in FCM measured FLS and SS in the HL + Si-treated samples over the untreated controls. Modest increases in cell sizes and in Chl *a* were also observed for PRO, PEUK and MICRO-EUK in the HL + Si-treated samples indicating a net positive impact of Si on phytoplankton growth in the CRD.

Although little is known about the biochemistry of Si uptake and cellular processes involved in its use in PICO phytoplankton, our observations of enhanced growth of both small and large phytoplankton in the HL + Si treatments seem to suggest that Si uptake is a light-dependent process.

These observations are consistent with reports of significant reductions in Si uptake rates during the dark phase of a diel cycle (Goering *et al.*, 1973; Leynaert *et al.*, 2001). Observations of maximum net rates of biogenic Si production at shallower depths during our cruise (Krause *et al.*, 2016) are also consistent with this interpretation. These observations of light dependency of Si uptake by phytoplankton in the CRD contrast, however, with reports of little evidence of systematic day/night differences in biogenic production rates of natural phytoplankton populations (Brzezinski and Nelson, 1989; Nelson and Brzezinski, 1997). This discrepancy might be explained by results suggesting that Si uptake can differ considerably among species (Wheeler *et al.*, 1983; Putt and Prézelin, 1988; Kröger *et al.*, 2000).

Another possible reason for the enhanced response of CRD phytoplankton to HL + Si can be attributed to possible photochemical release (Johnson *et al.*, 1994; Sunda and Huntsman, 1998) and enhanced bioavailability of colloid-bound trace metals (Bruland, 1989; Lohan *et al.*, 2002; Morel and Price, 2003; Saito *et al.*, 2005, 2008; Mioni *et al.*, 2007). That is, increased availability of trace metals due to photochemical release could have contributed to enhanced Si uptake under HL conditions.

Our results of Fe and Zn-induced increases in phytoplankton Chl *a* content and growth in all groups of phytoplankton are consistent with previous observations in the CRD (Saito *et al.*, 2005) and those of Chappell *et al.* (2016). What is novel about our observations, however, is the finding of an increase in cell numbers and biomass of PICO as well as the increases in cell size of SYN in the HL + Si-treated samples. Neither Si nor Si/light co-limitation have been reported for PICO or for NANO + MICRO from the CRD, nor have previous studies documented specific requirements for Si by PRO, SYN or PEUK or enhancement of their growth rates by Si. Nonetheless, the observed response of PICO to Si could be relevant to the enigmatic nature of the Si cycle in the CRD, which has among the highest rates of biogenic silica export recorded for tropical open ocean water ecosystems, despite low standing stocks of diatoms (Honjo *et al.*, 2008; Stukel *et al.*, 2013; Krause *et al.*, 2016). Our results support the notion that Si concentrations in the CRD are suboptimal for MICRO-EUK, and consequently for diatoms that are part of this size fraction in CRD waters. While observations of enhanced NANO + MICRO Chl *a* in the +Si treatments are not surprising, given the reported Si limitation of diatoms in the Equatorial Pacific (Ku *et al.*, 1995; Dugdale *et al.*, 2011), what is surprising are observations of Si-mediated increases in PICO-sized cells, which suggest that Si limitation may be more widespread in the CRD than previously recognized.

Unlike other experimental responses, PICO Chl *a* enhancements in the HL + Si treatments were consistent

across all experiments, suggesting potential light and Si co-limitation of CRD picophytoplankton. In Cycles 2 and 3, the accumulation of PICO Chl *a* in the HL + Si treatments rivaled that of the NANO + MICRO fraction. In Cycle 3, the increase in PICO Chl *a* in the HL + Si treatment by Day 8 accounted for almost 95% of the increase in total Chl *a*, and FCM analyses revealed that SYN, PRO and PEUK populations all contributed to this increase. In other experiments however, the results for these groups were not so obvious, and sometimes even qualitatively opposite to those recorded for PICO Chl *a*. Such results, combined with the substantial increases and decreases of populations during the incubations, suggest that predator–prey oscillations might keep population abundances in check, even when Chl *a* registers a physiological or cell size response.

Although several strains of SYN and PEUK are known to grow well in high-light, low-nutrient environments (Kana and Glibert, 1987), there are no data to support the idea that growth of non-Si cell-walled phytoplankton such as SYN, PRO and PEUK may be co-limited by Si, nor are there known biochemical mechanisms that link SYN to Si-rich environments. What has become recently known however through SXRF analysis (Baines *et al.*, 2012) is that even organisms, like SYN that do not have a specific biochemical requirement for Si, are capable of accumulating this element within their cells. There is no comparable information for PRO, but conspicuous increases in SYN cell sizes (based on FCM measurements of SS) and to a certain extent PRO cell sizes in the HL + Si treatments suggest that PICO could play a broader role in Si cycling than previously appreciated. If this is true, the total amount of biogenic silica (bSi) associated with picophytoplankton in the CRD, even if not impressive on a biomass-specific basis, could be very substantial, since picophytoplankton comprise the majority of phytoplankton biomass in the region while diatoms represent only ~1% (Taylor *et al.*, 2016). Understanding the role of PICO in the CRD Si cycle might therefore help resolve the Si paradox of the CRD, comprised of a small diatom population, but with one of the highest rates of biogenic Si export in tropical open-ocean systems (Honjo *et al.*, 2008; Krause *et al.*, 2016).

Our findings could also have implications for understanding the cycling of Si-associated bio-reactive elements in the upper oceans, which have long been thought to be mainly regulated by diatoms and larger phytoplankton (Martin-Jézéquel *et al.*, 2000). For example, nitrate-based new production and carbon and nitrogen export out of the euphotic zone are generally observed to be high when surface-bloom populations are dominated by diatoms. More recent studies have noted, however, that PICO, typically considered less efficient in export, can be disproportionately represented in the material that settles into sediment traps beneath the euphotic zone (Amacher *et al.*, 2009, 2013). In the CRD, the biomass dominance by picophytoplankton (notably SYN), the non-trivial accumulation of Si in SYN (Baines *et al.*, 2012) and potentially in PRO, and our observations of Si stimulation of PICO in general, combine to suggest a potentially significant role of small phytoplankton in export processes.

ACKNOWLEDGEMENTS

The authors would like to gratefully acknowledge the support of late Dr Toshiro Saino (JAMSTEC) Japan for use of his FRRF and for many helpful discussions concerning measurements of phytoplankton photophysiology. We are thankful to undergraduate students Kelly Keebler (Bowdoin College, Maine) and Allison Brandeis (Colby College) for their invaluable help with sample collections, onboard experiments and sample processing. We also thank Drs Jim Moffett and Jagruti Vedamati (Univ. Southern California), Dreux Chappell (Old Dominion Univ.) for help with the collection of trace metal contamination-free samples and use of their facilities. We are also grateful to Captain Christopher Curl, resident technicians and the crew aboard the *RV* Melville for excellent support of our research.

FUNDING

This component of the CRD Flux and Zinc Experiments study was supported by US National Science Foundation grants OCE-112103 to J.I.G. and -0826626 to M.R.L. Internship support for Kelly Keebler from Bowdoin College, Brunswick, Maine, and for Allison Brandeis from Colby College, Lewiston, Maine, from the Maine Space Grants Consortium is also gratefully acknowledged.

REFERENCES

Ahlgren, N. A., Noble, A., Patton, A. P., Roache-Johnson, K., Jackson, L., Robinson, D., McKay, C., Moore, L. R. *et al.* (2014) The unique trace metal and mixed layer conditions of the Costa Rica upwelling dome support a distinct and dense community of *Synechococcus*. *Limnol. Oceanogr.*, **59**, 2166–2184.

Amacher, J., Neuer, S., Anderson, I. and Massana, R. (2009) Molecular approach to determine contributions of the protist community to particle flux. *Deep-Sea. Res. I*, **56**, 2206–2215.

Amacher, J., Neuer, S. and Lomas, M. (2013) DNA-based molecular fingerprinting of eukaryotic protists and cyanobacteria contributing to sinking particle flux at the Bermuda Atlantic time-series study. *Deep-Sea. Res. II*, **93**, 71–83.

Baines, S. B., Twining, B. S., Brzezinski, M. A., Krause, J. W., Vogt, S., Assael, D. and McDaniel, H. (2012) Significant silicon accumulation by marine picocyanobacteria. *Nat. Geosci.*, **5**, 886–891.

Baines, S. B., Twining, B. S., Vogt, S., Balch, W. M., Fisher, N. S. and Nelson, D. M. (2011) Elemental composition of equatorial Pacific diatoms exposed to additions of silicic acid and iron. *Deep-Sea Res. II*, **58**, 512–523.

Bruland, K. W. (1989) Complexation of zinc by natural organic ligands in the central North Pacific. *Limnol. Oceanogr.*, **34**, 269–285.

Bruland, K. W., Rue, E. L., Smith, G. J. and DiTullio, G. R. (2005) Iron, macronutrients and diatom blooms in the Peru upwelling regime: brown and blue waters of Peru. *Mar. Chem.*, **93**, 81–103.

Brzezinski, M. A., Baines, S., Balch, W. M., Beucher, C. P., Chai, F., Dugdale, R. C., Krause, J. W., Landry, M. R. *et al.* (2011) Colimitation of diatoms by iron and silicic acid in the equatorial Pacific. *Deep-Sea Res. II*, **58**, 493–511.

Brzezinski, M. A., Dumousseaud, C., Krause, J. W., Measures, C. I. and Nelson, D. M. (2008) Iron and silicic acid concentrations together regulate Si uptake in the equatorial Pacific Ocean. *Limnol. Oceanogr.*, **53**, 875–889.

Brzezinski, M. A. and Nelson, D. M. (1989) Seasonal changes in the silicon cycle within a Gulf Stream warm-core ring. *Deep-Sea Res. I*, **36**, 1009–1030.

Chappell, P. D., Jagruti, V., Selph, K. A., Cyr, H. A., Jenkins, B. D., Landry, M. R. and Moffett, J. W. (2016) Preferential depletion of zinc within Costa Rica Upwelling Dome creates conditions for zinc co-limitation of primary production. *J. Plankton Res.*, **38**, 244–255.

Davey, E. W., Gentile, J. H., Erickson, S. J. and Betzer, P. (1970) Removal of trace metals from marine culture media. *Limnol. Oceanogr.*, **15**, 486–488.

Décima, M., Landry, M. R., Stukel, M. R., Lopez-Lopez, L. and Krause, J. W. (2016) Mesozooplankton biomass and grazing in the Costa Rica Dome: amplifying variability through the plankton food web. *J. Plankton Res.*, **38**, 317–330.

Dugdale, R. C., Chai, F., Feely, R. A., Measures, C. I., Parker, A. E. and Wilkerson, F. P. (2011) The regulation of equatorial Pacific new production and pCO_2 by silicate-limited diatoms. *Deep-Sea Res. II*, **58**, 477–492.

Fiedler, P. C. (2002) The annual cycle and biological effects of the Costa Rica Dome. *Deep-Sea Res. I*, **49**, 321–338.

Franck, V. M., Bruland, K. W., Hutchins, D. A. and Brzezinski, M. A. (2003) Iron and zinc effects on silicic acid and nitrate uptake kinetics in three high-nutrient, low-chlorophyll (HNLC) regions. *Mar. Ecol. Prog Ser.*, **252**, 15–33.

Freibott, A., Taylor, A. G., Selph, K. E., Liu, H., Zhang, W. and Landry, M. R. (2016) Biomass and composition of protist grazers and heterotrophic bacteria in the Costa Rica Dome during summer 2010. *J. Plankton Res.*, **38**, 230–243.

Fujiki, T., Matsumoto, K., Watanabe, S., Hosaka, T. and Saino, T. (2011) Phytoplankton productivity in the western subarctic gyre of the North Pacific in early summer 2006. *J. Oceanogr.*, **3**, 295–303.

Goering, J. J., Nelson, D. M. and Carter, J. A. (1973) Silicic acid uptake by natural populations of marine phytoplankton. *Deep Sea Res.*, **20**, 777–789.

Gordon, L. I., Jennings, J., Ross, J. C. and Krest, J. M. (1992) A suggested protocol for continuous flow automated analysis of seawater nutrients (phosphate, nitrate, nitrite and silicic acid) in the WOCE Hydrographic Program and the Joint Global Ocean Fluxes Study Group. Chemical Oceanography Group, Oregon State Univ., College of Oceanography, Oregon, USA, Vol. Tech. Rpt. 92-1.

Gutiérrez-Rodríguez, A., Selph, K. E. and Landry, M. R. (2016) Phytoplankton growth and microzooplankton grazing dynamics across vertical environmental gradients determined by transplant *in situ* dilution experiments. *J. Plankton Res.*, **38**, 271–289.

Gutiérrez-Rodríguez, A., Slack, G., Daniels, E. F., Selph, K. E., Palenik, B. and Landry, M. R. (2014) Fine spatial structure of genetically distinct picocyanobacterial populations across environmental gradients in the Costa Rica Dome. *Limnol. Oceanogr.*, **59**, 705–723.

Hofmann, E. E., Busalacchi, A. J. and O'Brien, J. J. (1981) Wind generation of the Costa Rica Dome. *Science*, **214**, 552–554.

Honjo, S., Manganini, S. J., Krishfield, R. A. and Francois, R. (2008) Particulate organic carbon fluxes to the ocean interior and factors controlling the biological pump: a synthesis of global sediment trap programs since 1983. *Prog. Oceanogr.*, **76**, 217–285.

Hutchins, D. A. and Bruland, K. W. (1998) Iron-limited diatom growth and Si:N uptake ratios in a coastal upwelling regime. *Nature*, **393**, 561–564.

Johnson, K. S., Coale, K. H., Elrod, V. A. and Tindale, N. W. (1994) Iron photochemistry in seawater from the equatorial Pacific. *Mar. Chem.*, **46**, 319–334.

Kana, T. M. and Glibert, P. M. (1987) Effect of irradiances up to 2000 $\mu E\ m^{-2}\ s^{-1}$ on marine *Synechococcus* WH7803. I. Growth, pigmentation, and cell composition. *Deep-Sea Res. A*, **34**, 479–495.

Key, T., Mccarthy, A., Campbell, D. A., Six, C., Roy, S. and Finkel, Z. V. (2010) Cell size trade-offs govern light exploitation strategies in marine phytoplankton. *Environ. Microbiol.*, **12**, 95–104.

Kolber, Z. and Falkowski, P. G. (1993) Use of active fluorescence to estimate photosynthesis in-situ. *Limnol. Oceanogr.*, **38**, 1646–1665.

Krause, J. W., Stukel, M. R., Taylor, A. G., Taniguchi, D. A., De Verneil, A. and Landry, M. R. (2016) Net biogenic silica production and the contribution of diatoms to new production and organic matter export in the Costa Rica Dome ecosystem. *J. Plankton Res.*, **38**, 216–229.

Kröger, N., Deutzmann, R., Bergsdorf, C. and Sumper, M. (2000) Species-specific polyamines from diatoms control silica morphology. *Proc. Natl Acad. Sci. USA*, **97**, 14133–14138.

Ku, T.-L., Luo, S., Kusakabe, M. and Bishop, J. K. B. (1995) ^{228}Ra-derived nutrient budgets in the upper equatorial Pacific and the role of "new" silicate in limiting productivity. *Deep-Sea Res. II*, **42**, 479–497.

Lam, P. J., Tortell, P. D. and Morel, F. M. (2001) Differential effects of iron additions on organic and inorganic carbon production by phytoplankton. *Limnol. Oceanogr.*, **46**, 1199–1202.

Landry, M. R., Verneil, A. D., Goes, J. I. and Moffett, J. W. (2016a) Plankton dynamics and biogeochemical fluxes in the Costa Rica Dome: introduction to CRD Flux and Zinc Experiments. *J. Plankton Res.*, **38**, 167–182.

Landry, M. R., Selph, K. E., Décima, M., Gutiérrez-Rodríguez, A., Stukel, M. R., Taylor, A. G. and Pasulka, A. L. (2016b) Phytoplankton production and grazing balances in the Costa Rica Dome. *J. Plankton Res.*, **38**, 366–379.

Leblanc, K., Hare, C. E., Boyd, P. W., Bruland, K. W., Sohst, B., Pickmere, S., Lohan, M. C., Buck, K. *et al.* (2005) Fe and Zn effects on the Si cycle and diatom community structure in two contrasting high and low-silicate HNLC areas. *Deep Sea Res. I*, **52**, 1842–1864.

Leynaert, A., Tréguer, P., Lancelot, C. and Rodier, M. (2001) Silicon limitation of biogenic silica production in the Equatorial Pacific. *Deep Sea Res. I*, **48**, 639–660.

Li, W. K. W. and Harrison, W. G. (1982) Carbon flow into the end-products of photosynthesis in short and long incubations of a natural phytoplankton population. *Mar. Biol.*, **72**, 175–182.

Li, W. K. W., Subba Rao, D. V., Harrison, W. G., Smith, J. C., Cullen, J. J., Irwin, B. and Platt, T. (1983) Autotrophic picoplankton in the tropical ocean. *Science*, **219**, 292–295.

Lohan, M. C., Statham, P. J. and Crawford, D. W. (2002) Total dissolved zinc in the upper water column of the subarctic North East Pacific. *Deep-Sea Res. II*, **49**, 5793–5808.

Martin-Jézéquel, V., Hildebrand, M. and Brzezinski, M. A. (2000) Silicon metabolism in diatoms: implications for growth. *J. Phycol.*, **36**, 821–840.

Mioni, C. E., Pakulski, J., Poorvin, L., Baldwin, A., Twiss, M. R., Jeffrey, W. H. and Wilhelm, S. W. (2007) Variability in the *in situ* bioavailability of Fe to bacterioplankton communities in the eastern subtropical Pacific Ocean. *Aquat. Microb. Ecol.*, **46**, 239.

Monger, B. C. and Landry, M. R. (1993) Flow cytometric analysis of marine bacteria with Hoechst 33342. *Appl. Environ. Microbiol.*, **59**, 905–911.

Morel, F. M. M. and Price, N. M. (2003) The biogeochemical cycles of trace metals in the oceans. *Science*, **300**, 944–947.

Nelson, D. M. and Brzezinski, M. A. (1997) Diatom growth and productivity in an oligotrophic midocean gyre: a 3-yr record from the Sargasso Sea near Bermuda. *Limnol. Oceanogr.*, **42**, 473–486.

Olson, R. J., Sosik, H. M., Chekalyuk, A. M. and Shalapyonok, A. (2000) Effects of iron enrichment on phytoplankton in the Southern Ocean during late summer: active fluorescence and flow cytometric analyses. *Deep Sea Res. II.*, **47**, 3181–3200.

Putt, M. and Prézelin, B. B. (1988) Diel periodicity of photosynthesis and cell division compared in *Thalassiosira weissflogii* (Bacillariophyceae). *J. Phycol.*, **24**, 315–324.

Ryan-Keogh, T. J., Macey, A. I., Nielsdóttir, M. C., Lucas, M. I., Steigenberger, S. S., Stinchcombe, M. C. and Moore, C. M. (2013) Spatial and temporal development of phytoplankton iron stress in relation to bloom dynamics in the high-latitude North Atlantic Ocean. *Limnol. Oceanogr.*, **58**, 533–545.

Saito, M. A., Goepfert, T. J. and Ritt, J. T. (2008) Some thoughts on the concept of colimitation: Three definitions and the importance of bioavailability. *Limnol. Oceanogr.*, **53**, 276–290.

Saito, M. A. and Moffett, J. W. (2002) Temporal and spatial variability of cobalt in the Atlantic Ocean. *Geochim. Cosmochim. Acta*, **66**, 1943–1953.

Saito, M. A., Rocap, G. and Moffett, J. W. (2005) Production of cobalt binding ligands in a *Synechococcus* feature at the Costa Rica upwelling dome. *Limnol. Oceanogr.*, **50**, 279–290.

Selph, K. E., Landry, M. R., Taylor, A. G., Gutiérrez-Rodríguez, A., Stukel, M. R., Wokuluk, J. and Pasulka, A. (2016) Phytoplankton production and taxon-specific growth rates in the Costa Rica Dome. *J. Plankton Res.*, **38**, 199–215.

Stukel, M. R., Benitez-Nelson, C. R., Décima, M., Taylor, A. G., Buchwald, C. and Landry, M. R. (2016) The biological pump in the Costa Rica Dome: an open ocean upwelling system with high new production and low export. *J. Plankton Res.*, **38**, 348–365.

Stukel, M. R., Décima, M., Selph, K. E., Taniguchi, D. A. A. and Landry, M. R. (2013) The role of Synechococcus in vertical flux in the Costa Rica upwelling dome. *Prog. Oceanogr.*, **112–113**, 49–59.

Suggett, D. J., Moore, C. M., Hickman, A. E. and Geider, R. J. (2009) Interpretation of fast repetition rate (FRR) fluorescence: signatures of phytoplankton community structure versus physiological state. *Mar. Ecol. Prog. Ser.*, **376**, 1–19.

Sunda, W. G. and Huntsman, S. A. (1995) Iron uptake and growth limitation in oceanic and coastal phytoplankton. *Mar. Chem.*, **50**, 189–206.

Sunda, W. G. and Huntsman, S. A. (1998) Processes regulating cellular metal accumulation and physiological effects: phytoplankton as model systems. *Sci. Total Environ.*, **219**, 165–181.

Takeda, S. (1998) Influence of iron availability on nutrient consumption ratio of diatoms in oceanic waters. *Nature*, **393**, 774–777.

Taylor, A. G., Landry, M. R., Selph, K. E. and Gutiérrez-Rodríguez, A. (2016) Patterns of microbial community biomass, composition and HPLC diagnostic pigments in the Costa Rica upwelling dome. *J. Plankton Res.*, **38**, 183–198.

Tortell, P. D., DiTullio, G. R., Sigman, D. M. and Morel, F. M. (2002) CO_2 effects on taxonomic composition and nutrient utilization in an Equatorial Pacific phytoplankton assemblage. *Mar. Ecol. Prog. Ser.*, **236**, 37–43.

Umatani, S. and Yamagata, T. (1991) Response of the Eastern Tropical Pacific to meridional migration of the ITCZ: the generation of the Costa Rica Dome. *J. Phys. Oceanogr.*, **21**, 346–363.

Vassiliev, I. R., Kolber, Z., Wyman, K. D., Mauzerall, D., Shukla, V. K. and Falkowski, P. G. (1995) Effects of iron limitation on photosystem II composition and light utilization in *Dunaliella tertiolecta*. *Plant Physiol.*, **109**, 963–972.

Vedamati, J. (2013) Comparative behavior and distribution of biologically relevant trace metals, iron, manganese and copper in four representative oxygen deficient regimes of the world's oceans. PhD (Ocean Sciences) dissertation, University of Southern California, August 2013, 236 pp.

Wheeler, P. A., Olson, R. J. and Chisholm, S. W. (1983) Effects of photocycles and periodic ammonium supply on three marine phytoplankton species. II. Ammonium uptake and assimilation. *J. Phycol.*, **19**, 528–533.

Wyrtki, K. (1964) Upwelling in the Costa Rica Dome. *Fish. Bull.*, **63**, 355–372.